UDK 549.67:544.032.53
Original scientific article/Izvirni znanstveni članek

ISSN 1580-2949
Mater. Tehnol.

A BIFUNCTIONAL Fe_3O_4@ZEOLITE MAGNETIC COMPOSITE DESIGNED VIA A SYNERGISTIC DUAL-SITE MECHANISM FOR THE EFFIACIENT AND SIMULTANEOUS REMOVAL OF AMMONIA NITROGEN AND PHOSPHATE FROM RURAL DOMESTIC SEWAGE

DVOFUNKCIONALNI MAGNETNI KOMPOZIT NA OSNOVI MAGNETITA IN ZEOLITA, ZASNOVAN S SINERGISTIČNIM DVOJNIM MEHANIZMOM ZA UČINKOVITO IN SOČASNO ODSTRANJEVANJE AMONIJAKA IN FOSFATA IZ PODEŽELSKIH DOMAČIH ODPLAK

Xiankun Zhu[1,2]*

[1]Shanghai Investigation, Design & Research Institute Co., Ltd., Shanghai 200335, China
[2]Three Gorges Smart Water Technology Co., Ltd., Shanghai 200335, China

Prejem rokopisa – received: 2025-10-17; sprejem za objavo – accepted for publication: 2026-01-09

doi:10.17222/mit.2025.1593

Developing efficient materials for the simultaneous removal of nitrogen (N) and phosphorus (P) from rural domestic sewage is critical for eutrophication control. This study constructed a bifunctional Fe_3O_4@Zeolite magnetic composite via a hydrothermal method to achieve this goal. Characterization results confirmed the uniform loading of Fe_3O_4 nanoparticles onto the zeolite framework. The composite demonstrated excellent simultaneous removal performance at neutral pH (6.0–7.0), achieving 83.6 % ammonia nitrogen (NH_4^+-N) and 81.2 % phosphate (PO_4^{3-}-P) removal. The adsorption followed pseudo-second-order kinetics with rapid equilibrium (60 min). The Langmuir isotherm model indicated maximum adsorption capacities of 23.5 mg/g for NH_4^+-N and 21.6 mg/g for PO_4^{3-}-P. Mechanistic analysis via XPS revealed a distinct "site-specific" synergy: NH_4^+-N was captured via ion exchange with the zeolite lattice, while PO_4^{3-}-P formed stable inner-sphere complexes (Fe-O-P) with Fe_3O_4 nanoparticles. The adsorption process was spontaneous ($\Delta G° < 0$) and endothermic ($\Delta H° < 0$). Furthermore, the composite exhibited excellent magnetic separability and reusability, retaining over 88 % of its initial efficiency after five regeneration cycles. It also effectively treated real rural sewage, validating its engineering potential as a robust, multifunctional environmental material.

Keywords: magnetic nanocomposite material, Fe_3O_4@Zeolite, ammonia nitrogen removal, phosphate removal

Razvoj učinkovitih materialov za sočasno odstranjevanje dušika (N) in fosforja (P) iz podeželskih gospodinjskih odplak je ključnega pomena za nadzor evtrofikacije. To je proces večanja količine biomase v vodi kot posledica povečane koncentracije anorganskih hranil (npr.: nitratov in fosfatov) v ekosistemu. Za ta namen, so avtorji s hidrotermalno metodo izdelali dvofunkcionalni magnetni kompozit na osnovi magnetita (Fe_3O_4) in zeolita (skupina več vrst vulkanskih mikroporoznih kristaliničnih alumo-silikatnih mineralov). Avtorji članka so izvedli karakterizacijo izdelanega magnetnga nanokompozita. Z njo so potrdili enakomerno nalaganje nanodelcev Fe_3O_4 na zeolitno ogrodje. S kompozitom so dosegli odlično (83,6 %) sočasno odstranjevanje amonijevega dušika NH_4^+-N in 81,2 % fosfata PO_4^{3-}-P pri nevtralnem pH (6,0–7,0). Kinetika adsorpcije psevdo-drugega reda je potekala zelo hitro z ravnotežjem po 60 minutah. Langmuirov izotermni model je pokazal največjo adsorpcijsko kapaciteto 23,5 mg/g za NH_4^+-N in 21,6 mg/g za PO_4^{-3}-P. Mehanistična analiza z XPS je pokazala izrazito "lokacijsko specifično" sinergijo; NH_4^+-N je bil zajel z ionsko izmenjavo z zeolitno mrežo, medtem ko je PO_4^{3-}-P tvoril stabilne komplekse notranje sfere (Fe-O-P) z nanodelci Fe_3O_4. Proces adsorpcije je bil spontan ($\Delta G°<0$) in endotermen ($\Delta H°<0$). Poleg tega je kompozit pokazal odlično magnetno ločljivost in ponovno uporabnost, saj je po petih regeneracijskih ciklih ohranil več kot 88 % svoje začetne učinkovitosti. Učinkovito je čistil tudi prave podeželske odplake, kar potrjuje njegov inženirski potencial za uporabo kot robustni, večnamenski okoljski material.

Ključne besede: magnetni nanokompozit, Fe_3O_4 in zeolit, odstranitev amonijevega dušika in fosfata

1 INTRODUCTION

As the economy in rural areas of China experiences rapid development and living standards improve, the discharge volume of rural domestic sewage increases year by year. This type of sewage generally contains high concentrations of nitrogen (N) and phosphorus (P) nutrients. If discharged directly without treatment, it will lead to the eutrophication of surface-water bodies, posing a severe threat to drinking-water safety and the regional ecological balance.[1–3] Therefore, developing efficient and low-cost technologies to remove N and P from rural domestic sewage stands as a crucial subject within the contemporary realm of water-environment management.[4,5]

At present, the predominant technologies for N and P removal encompass chemical precipitation, biological treatment processes, and adsorption techniques. Although chemical precipitation is effective, it has drawbacks such as high reagent costs and the generation of large amounts of chemical sludge.[6] Biological methods

*Corresponding author's e-mail:
zxk_kunkk@sina.com (Xiankun Zhu)

© 2026 The Author(s). Except when otherwise noted, articles in this journal are published under the terms and conditions of the Creative Commons Attribution 4.0 International License (CC BY 4.0).

are sensitive to operating conditions and lack stability in decentralized rural-sewage treatment scenarios.[7,8] In comparison, the adsorption method attracts significant attention due to its advantages of simple operation, rapid reaction, and environmental friendliness. Natural zeolite, with its inherent cation-exchange capacity (CEC), is considered a promising material for removing ammonia nitrogen (NH_4^+-N).[9,10] However, its adsorption capacity is limited, and it has virtually no removal ability for anions such as phosphate (PO_4^{3-}-P). Additionally, difficulties in solid-liquid separation after treatment also restrict its application.[11]

To overcome these limitations, material modification has become a research focus. Among various strategies, the introduction of nanoscale magnetic iron oxides (such as Fe_3O_4) is a highly attractive strategy, as it not only provides abundant adsorption sites for PO_4^{3-}-P but also imparts magnetic responsiveness to the material, simplifying the solid-liquid separation process.[12,13] Although previous studies have explored loading Fe_3O_4 onto porous carriers, most of them have focused on the removal of a single pollutant or conducted evaluations in idealized pure-water systems.[14] However, in complex rural sewage matrices characterized by high ionic strength and the coexistence of NH_4^+-N and PO_4^{3-}-P, the competitive adsorption behavior between these pollutants remains inadequately elucidated. Specifically, there is a lack of direct evidence at the atomic and chemical bond levels revealing the selective adsorption of two distinct pollutants at different functional sites on a single material. This lack of mechanistic clarity limits the transition of material design from empirical trials to precise functional engineering.

Therefore, this study aims to construct a bifunctional Fe_3O_4@Zeolite magnetic composite and systematically investigate its performance and mechanism. The core innovations are: (1) evaluating synchronous removal efficiency and selectivity under conditions simulating typical rural-sewage pollutant concentrations, and verifying its robustness against coexisting ions; (2) providing direct atomic-level evidence via X-ray photoelectron spectroscopy (XPS) for a "synergistic dual-site mechanism" combining zeolite ion exchange and Fe_3O_4 surface complexation; and (3) comprehensively assessing its engineering potential through coupled static-dynamic experiments and real wastewater verification.

2 METHODOLOGY

2.1 Laboratory chemicals and equipment

The natural zeolite utilized in the research was purchased from a mining company in Xinyang, Henan Province, and appeared as grayish-white porous granules. Its main physicochemical properties were as follows: a CEC of approximately 150 meq/100 g and a BET specific surface area of 45.2 $m^2\ g^{-1}$. After being crushed and sieved, granules with a particle size of 20-40 mesh were selected for the experiments. All the reagents required during the modification process were of analytical reagent (AR) grade, ensuring the repeatability and reliability of the experiments. The main reagents included: iron(III) chloride hexahydrate ($FeCl_3{\cdot}6H_2O$, purity ≥99 %, Sinopharm Chemical Reagent Co., Ltd.), ferrous sulfate heptahydrate ($FeSO_4{\cdot}7H_2O$, purity ≥99 %, Tianjin Damao Chemical Reagent Factory), ammonia solution (25 %, Aladdin), sodium hydroxide (NaOH, Sinopharm), hydrochloric acid (HCl, 37 %, Tianjin Kermel), and anhydrous ethanol (C_2H_5OH, purity ≥99 %, Shanghai Lingfeng). The deionized water utilized in the experiments was produced using a laboratory-grade pure-water system (Smart-Q30, Shanghai Hitech Instruments Co., Ltd.) with a conductivity of less than 0.1 μS cm^{-1}.

The main instruments used in the experiments included: an Ohaus-Toledo electronic balance (AR2140), a gas bath constant-temperature oscillator (SHZ-82) from Ronghua Instrument Manufacturing Co., Ltd., a Mettler-Toledo pH meter (FE20), and a constant-temperature drying oven (DGG-9070B) from Sunsine Test Instrument Co., Ltd. The equipment used for material characterization included: an X-ray diffractometer (XRD, model Bruker D8 Advance) manufactured by Bruker Corporation in Germany, a Fourier transform infrared spectrometer (FTIR, model Nicolet-460) produced by Thermo Fisher Scientific Inc., and an X-ray photoelectron spectrometer (XPS, model Escalab 250Xi) also manufactured by Thermo Fisher Scientific Inc.

2.2 Pretreatment of Zeolite

Natural zeolite often contains a certain amount of clay minerals, dust, and organic impurities. These impurities could block pores and affect the surface area, thereby reducing its adsorption performance. Therefore, it was essential to pretreat the zeolite before the experiments.[15,16] The specific method was as follows. The raw ore underwent multiple rounds of rinsing with deionized water until the resulting liquid was transparent and devoid of any suspended particles. After that, it was dried at 105 °C for 12 h to eliminate moisture and certain organic compounds. After drying, the zeolite was ground and then sieved through standard sieves to obtain granules with a size of 20-40 mesh for later use. The pretreated zeolite had unobstructed pores and an increased specific surface area, which facilitated the loading of Fe_3O_4 and the adsorption of N and P pollutants.

2.3 Synthesis of Fe_3O_4 nanoparticles

Nanoscale Fe_3O_4 was prepared using the chemical co-precipitation method. This method was characterized by its simple operation, high yield, and controllable particle size, making it suitable for large-scale preparation. The specific steps were as follows. First, solutions of $FeCl_3{\cdot}6H_2O$ and $FeSO_4{\cdot}7H_2O$ were prepared in a molar ratio of 2:1. These solutions were subsequently stirred

using a magnetic stirrer at 60 °C to guarantee the full dissolution and even distribution of the iron salts. Following this, the ammonia solution was slowly added dropwise, with constant stirring, to bring the solution's pH to approximately 10. As the pH increased, Fe^{2+} and Fe^{3+} ions co-precipitated to form black Fe_3O_4 nanoparticles. The precipitate was isolated with centrifugation and then rinsed successively with deionized water and absolute ethanol to eliminate any unreacted ions and residual by-products. Finally, it was dried at low temperature under a N atmosphere to obtain stable Fe_3O_4 powder. The nanoscale Fe_3O_4 prepared by this method typically had a particle size of 10–30 nm and exhibited good crystallinity and magnetic responsiveness.

2.4 Preparation of nano Fe_3O_4@Zeolite

To improve the adsorption capacity of zeolite for N and P, the synthesized nanoscale Fe_3O_4 was composited with the pretreated zeolite. The specific method was as follows: 10.0 g of pretreated zeolite particles were added to 500 mL of a nanoscale Fe_3O_4 suspension with a concentration of 1.0 g L^{-1}, and a hydrothermal treatment was carried out at 80 °C, lasting for about 12 h. During this process, Fe_3O_4 nanoparticles were anchored to the surface and within the pores of the zeolite through electrostatic attraction and interaction with surface hydroxyl groups, thereby forming the composite material Fe_3O_4@Zeolite. After repeated washing with deionized water until the conductivity of the supernatant stabilized and the pH reached neutrality, the product underwent drying at 60 °C and was then evenly ground. The resulting composite material combined the high specific surface area and CEC of zeolite with the magnetic separation performance and surface complexation capacity of Fe_3O_4, and was expected to significantly improve the removal efficiency of N and P. The detailed preparation procedure is depicted in **Figure 1** and comprised two core steps: (1) First, Fe^{2+} and Fe^{3+} precursor solutions were added dropwise to ammonia solution under stirring via the chemical co-precipitation method to generate a black suspension of nanoscale Fe_3O_4 particles; (2) Subsequently, the pretreated zeolite was added to this suspension, and a high-temperature hydrothermal reaction was conducted in a hydrothermal reactor to promote the stable loading of nanoscale Fe_3O_4 onto the surface and within the pore structures of the zeolite, ultimately yielding the Fe_3O_4@Zeolite composite material.

2.5 Characterization of modified materials

To verify the modification effects and gain an in-depth understanding of the material structure, various analytical techniques were employed for characterization in the study. XRD was employed to examine the crystal structure and phase makeup of the material, confirming the loading of Fe_3O_4 on the surface of the zeolite. FTIR was utilized to examine changes in the surface functional groups and assess the chemical bonding characteristics of zeolite before and after modification. Nitrogen adsorption-desorption isotherms were measured to determine the specific surface area using the Brunauer-Emmett-Teller (BET) method. The specific surface area of the Fe_3O_4@Zeolite composite was determined to be 39.6 m^2 g^{-1}, which represented a slight decrease compared to the raw zeolite (45.2 m^2 g^{-1}). This minor reduction is primarily attributed to the immobilization of dense Fe_3O_4 nanoparticles on the surface and the partial occupation of the zeolite's porous channels. However, the result indicates that the pore structure required for ion exchange was largely preserved during the hydrothermal modification. XPS was applied to analyze the elemental makeup and chemical oxidation states on the material surface before and after adsorption, focusing on

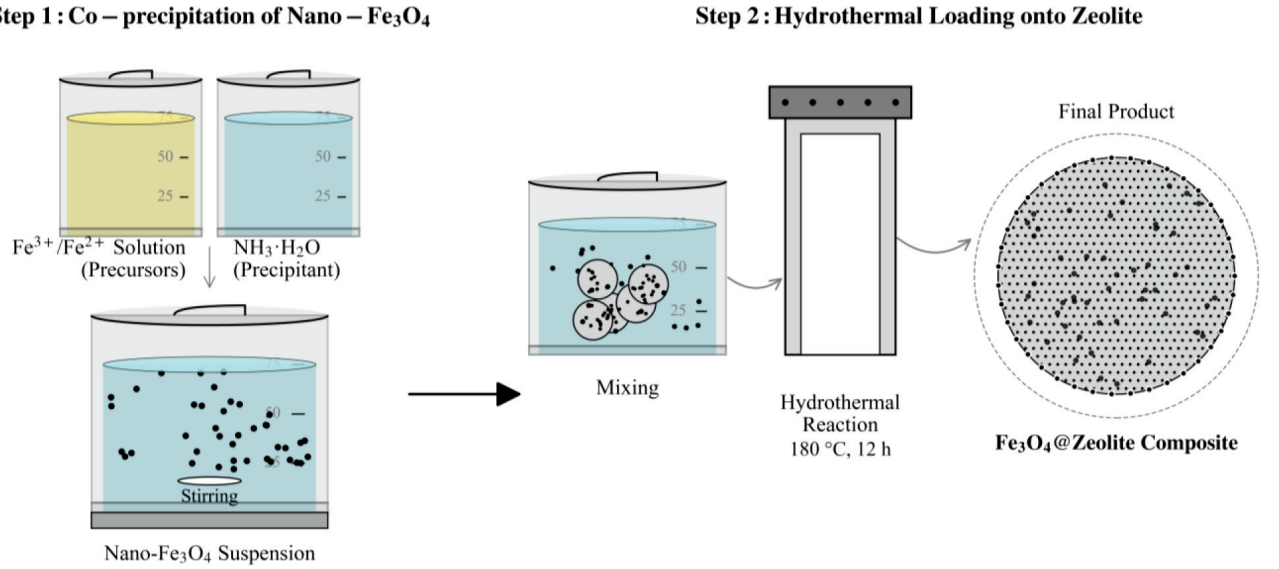

Figure 1: Preparation process for Fe_3O_4@Zeolite composite material

the fine spectra of Fe 2p, O 1s, N 1s, and P 2p, to elucidate the adsorption mechanism.[17–19]

2.6 Design of static adsorption experiment

Fe_3O_4@Zeolite was mixed with N-P solutions of certain concentrations and subjected to oscillatory reactions under different conditions of pH, reaction time, initial concentration, temperature, and coexisting ions. The NH_4^+-N concentration in the solution was measured via the Nessler's reagent spectrophotometric technique (HJ 535-2009), while the concentration of PO_4^{3-}-P (expressed as P) was measured by the molybdenum-antimony-antimony tartrate spectrophotometric method (GB 11893-89). Simulated wastewater was prepared by dissolving analytical grade ammonium chloride (NH_4Cl) and potassium dihydrogen phosphate (KH_2PO_4) in deionized water. In these fundamental kinetic and isotherm experiments, no additional background electrolytes were added to eliminate interference and accurately determine the intrinsic adsorption parameters of the material. The formulas for calculating the adsorption capacity and removal rate in the static experiments are shown in Equation (1).

$$\begin{cases} q_t = \dfrac{(C_0 - C_t)V}{m} \\ q_e = \dfrac{(C_0 - C_e)V}{m} \\ \eta = \dfrac{C_0 - C_t}{C_0} \end{cases} \quad (1)$$

In Equation (1), C_0 is the original concentration, C_t is the concentration at time t, C_e is the equilibrium concentration, V is the solution volume, m is the adsorbent mass, q_t and q_e are the instantaneous and equilibrium adsorption capacity respectively, and η is the removal rate. A diagrammatic illustration of the static adsorption experimental setup and timeline is shown in **Figure 2**. **Figure 2** illustrates the batch adsorption arrangement in conical flasks, including the mass of adsorbent added, placed on a gas-bath constant-temperature shaker. The initial pH was adjusted via a pH meter; samples were taken at predetermined time points, followed by rapid filtration/centrifugation to measure the concentration at each time point, with key time nodes marked accordingly.

2.7 Experimental design of dynamic column

An organic glass column, measuring 2.5 cm in diameter and 30 cm in height, was utilized to pack Fe_3O_4@Zeolite, simulating the operation of a permeable reactive barrier. Different hydraulic loading rates were set, with continuous influent water supply and effluent sampling. The removal effects of NH_4^+-N and P were detected, and the data were fitted through the Thomas and Yoon-Nelson models. The calculation formulas for the breakthrough ratio and the Thomas model are shown in Equation (2).

$$\begin{cases} B_t = \dfrac{C_{out}}{C_{in}} \\ \ln\left(\dfrac{C_{in}}{C_{out}} - 1\right) = k_{Th}\left(\dfrac{q_{Th}m}{Q} - C_{in}t\right) \end{cases} \quad (2)$$

In Equation (2), B_t is the penetration ratio. C_{in} and C_{out} are the inlet and outlet concentrations, Q is the flow rate, t is the operation time, k_{Th} is the Thomas rate constant, q_{Th} is the max adsorption capacity, and m is the mass of adsorbent. The diagrammatic illustration of the dynamic column experimental setup was shown in **Figure 3**. In **Figure 3**, the main body of the setup was an organic glass column measuring 2.5 cm in diameter and 30 cm in height, which was uniformly filled from bottom to top with nano Fe_3O_4@Zeolite as the adsorbent. During the experiment, simulated wastewater entered the column from the bottom via a constant-flow pump, fully contacted with the packing material after passing through the adsorption layer, and then flowed out from the top. The setup was equipped with sampling devices at the inlet and outlet for real-time detection of changes in the concentrations of NH_4^+-N and P, enabling the plotting of breakthrough curves and the analysis of kinetic characteristics.

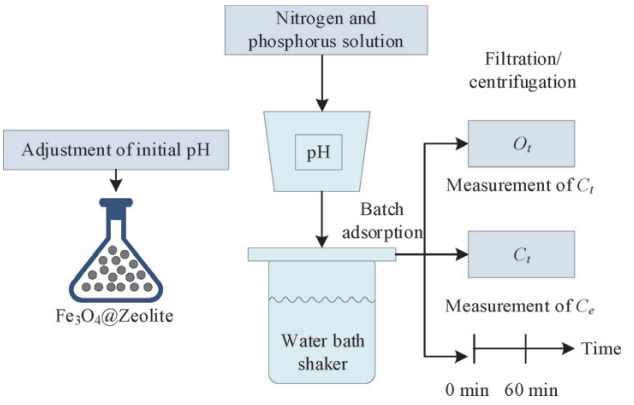

Figure 2: Illustration of static adsorption experimental device

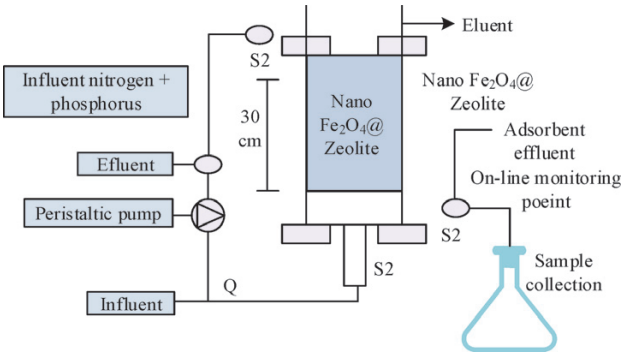

Figure 3: Illustration of dynamic column experimental device

2.8 Adsorption kinetics and isotherm analysis method

The data from the experiment were fitted through the pseudo-first-order and pseudo-second-order kinetic models to reveal the rate-controlling steps of N and P adsorption. The results of the isothermal adsorption experiments were fitted through the Langmuir and Freundlich models respectively to evaluate the max adsorption capacities of Fe_3O_4@Zeolite for N and P as well as the adsorption mechanisms. Furthermore, thermodynamic parameters (ΔG°, ΔH°, ΔS°) were computed to analyze the spontaneity, energy changes, and the nature of the adsorption process.[20–22] The pseudo-first-order kinetic model is presented as shown in Equation (3).

$$\ln(q_e - q_t) = \ln q_e - k_1 t \tag{3}$$

In Equation (3), k_1 is the pseudo-first-order kinetic rate constant. The pseudo-second-order dynamic model is shown in Equation (4).

$$\frac{t}{q_t} = \frac{1}{k_2 q_e^2} + \frac{t}{q_e} \tag{4}$$

In Equation (4), k_2 is the pseudo-second-order kinetic rate constant. The internal diffusion model is shown in Equation (5).

$$q_t = k_{id}\sqrt{t} + C_i \tag{5}$$

In Equation (5), k_{id} is the internal diffusion rate constant, and C_i is the intercept term, reflecting the external diffusion resistance. Langmuir model is shown in Equation (6).

$$\begin{cases} q_e = \dfrac{q_{max} K_L C_e)V}{1 + K_L C_e} \\ \dfrac{C_e}{q_e} = \dfrac{1}{K_L q_{max}} + \dfrac{C_e}{q_{max}} \end{cases} \tag{6}$$

In Equation (6), q_{max} is the max monolayer adsorption capacity under Langmuir hypothesis. K_L is the Langmuir affinity constant. Freundlich model is presented in Equation (7).

$$\begin{cases} q_e = K_F C_e^{1/n} \\ \ln q_e = \ln K_F + \dfrac{1}{n} \ln C_e \end{cases} \tag{7}$$

In Equation (7), K_F is the Freundlich capacity coefficient and n is the adsorption advantage index. In addition, the adsorption thermodynamic parameters are calculated by the distribution coefficient, as shown in Equation (8).

$$\begin{cases} \Delta G = -RT \ln K_d \\ \ln K_d = -\dfrac{\Delta H}{RT} + \dfrac{\Delta S}{R} \end{cases} \tag{8}$$

In Equation (8), K_d is the distribution coefficient, $\Delta G°$ is the standard free-energy change, $\Delta H°$ is the standard enthalpy change, and $\Delta S°$ is the standard entropy change. R and T are constants and temperatures, respectively.

2.9 Experiment on regeneration and recycling of adsorbent

To assess the sustainability and economic feasibility of Fe_3O_4@Zeolite in engineering applications, its regeneration performance was investigated. The saturated adsorbent (with a solid-to-liquid ratio of 1.0 g L^{-1}) was placed separately in 0.1 mol L^{-1} HCl, 0.1 mol L^{-1} NaOH, and 0.1 mol L^{-1} NaCl solutions and oscillated for desorption during 2 h at 298 K and 150 min^{-1}. After desorption, the adsorbent underwent multiple rinses with deionized water until the filtrate's pH reached neutral, after which it was dried at 60 °C for future application. This adsorption-desorption process was repeated for 5 cycles, and the stability and feasibility of its long-term application were assessed by comparing the retention rate of the adsorption capacity after each cycle.

2.10 Explanation of experimental design

All experiments (including batch adsorption and dynamic column experiments) were repeated three times, with the findings presented as mean ± standard deviation (mean ± SD). To quantify the performance enhancement brought about by Fe_3O_4 modification, experiments were set up using pretreated but unmodified zeolite as a control group, and parallel experiments were conducted under identical conditions.

2.11 Real rural-sewage experiment

2.11.1 Wastewater sampling and characterization

To assess the real-world applicability performance of the Fe_3O_4@Zeolite composite material, this study collected real rural domestic sewage. The water sample was collected at the entry point of a centralized domestic sewage-treatment station in a certain village. After collection, the water sample was first subjected to coarse filtration to remove large particulate suspended solids, and then filtered through a 0.45-μm microporous filter membrane to remove fine particles and micro-organisms. The resulting filtrate was refrigerated at 4 °C for later use. The filtered water sample was analyzed for water quality using standard methods, and its main physicochemical properties are shown in **Table 1**.

Table 1: Real rural-sewage quality parameters

Parameter	Unit	Content
pH	–	7.6 ± 0.2
Chemical oxygen demand (COD)	mg L^{-1}	185 ± 15
Total organic carbon (TOC)	mg L^{-1}	72 ± 8
NH_4^+-N	mg L^{-1}	38.2 ± 2.5
PO_4^{3-}-P	mg L^{-1}	6.1 ± 0.4
Ca^{2+}	mg L^{-1}	65.3
SO_4^{2-}	mg L^{-1}	95.8

2.11.2 Adsorption experiment

The aforementioned pretreated real rural sewage was taken and subjected to static adsorption experiments under the same optimal conditions as those used in the simulated wastewater experiments. The specific conditions were as follows: the dosage of Fe_3O_4@Zeolite was set to 1.0 g L^{-1}, a value determined to be optimal based on the preliminary dosage-optimization tests using simulated wastewater, balancing removal efficiency with material cost. The reaction took place in a temperature-controlled shaker at 298 K for a duration of 60 minutes. The solution's starting pH was set to 7.0 by adding dilute HCl or NaOH. After the reaction, samples were taken to measure the remaining concentrations of NH_4^+-N and PO_4^{3-}-P in the solution, and the removal rates were calculated. All experiments were conducted in triplicate.

3 OUTCOMES AND ANALYSIS

3.1 Characterization of physical and chemical properties of materials

To verify whether Fe_3O_4 nanoparticles were successfully loaded, a series of characterizations were conducted on the materials before and after modification (**Figures 4a-c**). As revealed by the XRD pattern in **Figure 4a**, the Fe_3O_4@Zeolite composite retained the characteristic diffraction peaks of zeolite, indicating that the crystal framework structure of zeolite remained stable during the modification process. Meanwhile, new diffraction peaks appeared at 2θ = 30.5°, 35.6°, 43.3°, 56.8°, and 62.4°, which fully corresponded to the (220), (311), (400), (511), and (440) crystal planes in the standard JCPDS card of magnetite Fe_3O_4, confirming that Fe_3O_4 had been successfully loaded in a crystalline phase. The EDS spectrum in **Figure 4b** showed that four main elements – Si, Al, O, and Fe – were present in the composite, with the mass fraction of Fe being approximately 14.12 %, further proving the successful introduction of iron. FTIR spectroscopy provided evidence at the chemical bond level for the successful incorporation of Fe_3O_4 (**Figure 4c**). Both spectra displayed vibration peaks of -OH at 3442 cm^{-1} and 1639 cm^{-1}, and exhibited the most typical asymmetric stretching vibration absorption peak of the Si-O-T framework of zeolite at ≈1083 cm^{-1}. The most prominent distinction was that the spectrum of Fe_3O_4@Zeolite exhibited a clear new absorption peak at approximately 576 cm^{-1}, which was absent in pure zeolite. This peak was assigned to the distinctive vibration of the Fe-O bond within the spinel framework, perfectly cross-verifying the XRD outcomes and confirming the successful loading of Fe_3O_4 from the perspective of functional groups. The aforementioned XRD, EDS, and FTIR results formed a complete chain of evidence, confirming the successful preparation of a structurally stable Fe_3O_4@Zeolite composite.

3.2 XPS analysis of PO_4^{3-}-P adsorption mechanism

To investigate the surface chemical properties and elucidate the adsorption mechanism, XPS analysis was conducted. **Figures 4d-g** present the detailed decon-

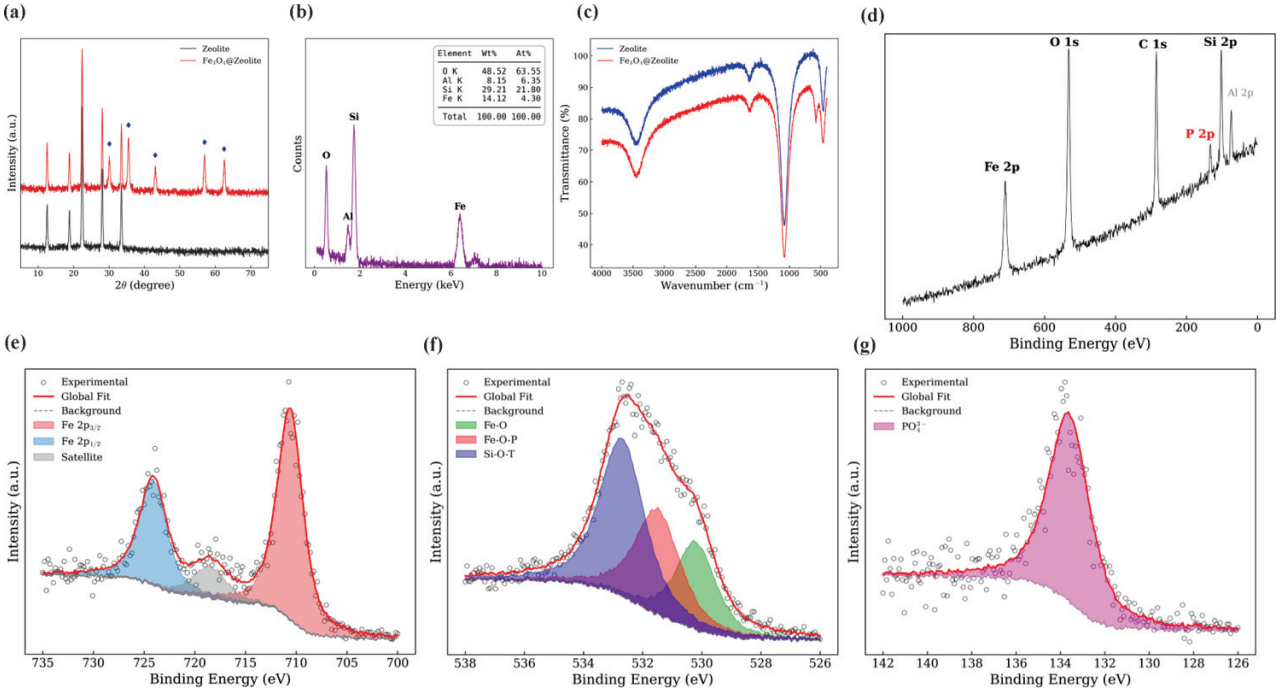

Figure 4: Results of material characterization including: a) XRD patterns of pure zeolite and Fe_3O_4@Zeolite, b) EDS spectrum and elemental composition of Fe_3O_4@Zeolite, c) FTIR spectra of pure zeolite and Fe_3O_4@Zeolite and d-g) XPS spectra of Fe_3O_4@Zeolite after PO_4^{3-}-P adsorption: d) Full survey spectrum, e) Fe 2p, f) O 1s, (g) P 2p

voluted spectra of the Fe_3O_4@Zeolite composite after phosphate adsorption. The survey spectrum (**Figure 4d**) clearly identifies the presence of P 2p (≈132 eV) alongside Fe, O, Si, Al, and C elements. Compared to the pristine material (spectrum not shown), the emergence of the distinct phosphorous signal provides direct evidence of PO_4^{3-} capture. The Fe 2p high-resolution spectrum (**Figure 4e**) confirms the stability of the iron oxide phase during the adsorption process. The spectrum exhibits the characteristic doublet of Fe $2p_{3/2}$ (≈710.4 eV) and Fe $2p_{1/2}$ (≈724.3 eV). Crucially, the satellite peak at ≈718.6 eV is clearly resolved, identifying the iron species as Fe_3O_4 with its specific Fe^{2+}/Fe^{3+} occupancy, rather than γ-Fe_2O_3. A detailed insight into the bonding mechanism is provided by the O 1s spectrum (**Figure 4f**). The distinct asymmetry of the peak necessitated fitting with three components: lattice oxygen (Fe-O) at ≈530.3 eV, the silica framework (Si-O-T) at ≈532.9 eV, and a specific intermediate component at ≈531.7 eV. This latter peak is attributed to the formation of Fe-O-P bonds, indicating that surface hydroxyl groups were consumed via ligand exchange to form inner-sphere complexes. This conclusion is further supported by the P 2p spectrum (**Figure 4g**), where the signal at ≈133.5 eV corresponds to the phosphate species bound to the metal oxide surface.

3.3 Comparison of adsorption performance and effect of pH

The solution pH was a critical factor influencing the adsorption process. As shown in **Figure 5**, this study compared the removal efficiencies of pollutants by the Fe_3O_4@Zeolite composite material and the unmodified zeolite control group under different pH conditions. The composite material exhibited optimal simultaneous removal performance for both pollutants within the neutral pH range of 6.0 to 7.0. In stark contrast, although the unmodified zeolite demonstrated NH_4^+-N removal efficiency comparable to that of the composite material due to its inherent CEC, its PO_4^{3-}-P removal capability was negligible (<5 %) across the entire pH range. This comparison decisively highlighted the crucial role of nano Fe_3O_4 as a specific adsorption site for PO_4^{3-}-P, confirming the success and necessity of the composite modification. For the composite material, when pH < 6, H^+ competed with NH_4^+ for ion exchange sites, leading to a decline in NH_4^+-N removal efficiency. However, when pH > 8, the removal efficiency for PO_4^{3-}-P decreased. This phenomenon can be explained by the surface charge properties of the iron oxides. The point of zero charge (PZC) for Fe_3O_4 typically lies between pH 6.5 and pH 7.5. At pH levels significantly above the PZC, the surface of the Fe_3O_4 nanoparticles becomes net negatively charged, resulting in strong electrostatic repulsion toward anionic phosphate species (PO_4^{3-}, HPO_4^{2-}). Simultaneously, the increased concentration of OH^- ions competed for the active iron sites, further inhibiting adsorption.

3.4 Adsorption kinetics analysis

The impact of reaction time on the adsorption process is illustrated in **Figure 6**. The adsorption amounts of NH_4^+-N and P rose swiftly in the initial 30 minutes and attained equilibrium around the 60-minute mark. The kinetic data were fitted using pseudo-first-order and pseudo-second-order models (**Table 2**). The results showed that the correlation coefficients (R^2) associated with the pseudo-second-order kinetic model were consistently above 0.99, and the computed equilibrium adsorption quantities (q_e, cal) closely aligned with the experi-

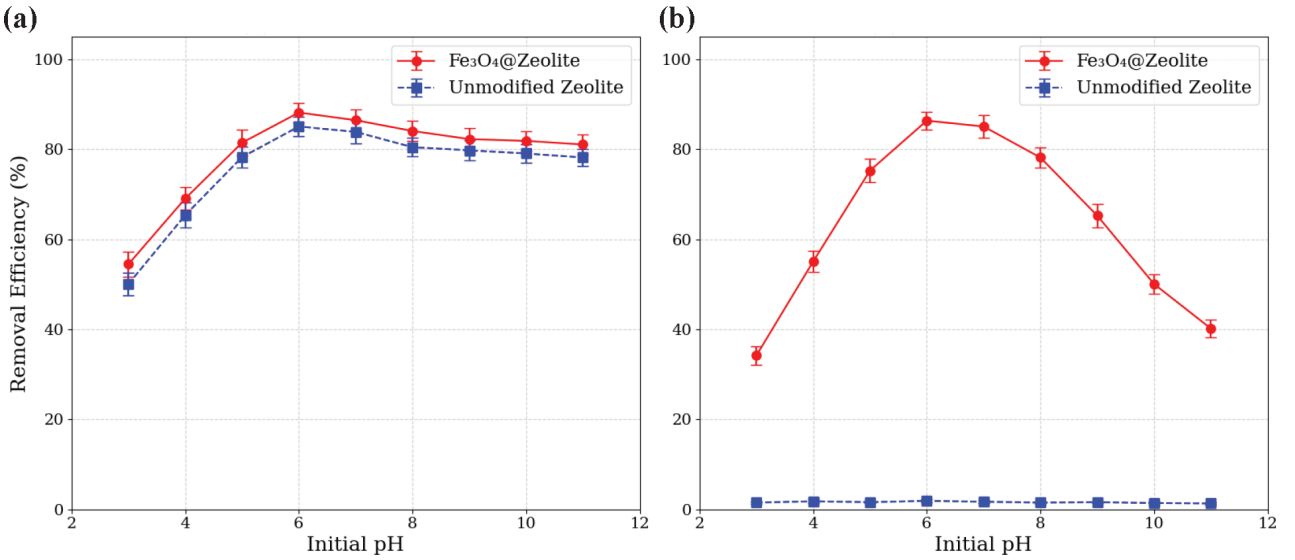

Figure 5: Comparison of (a) NH_4^+-N and (b) PO_4^{3-}-P removal efficiencies between Fe_3O_4@Zeolite and unmodified zeolite under different pH conditions

mentally observed values (q_e, exp). This indicated that the adsorption was mainly governed by chemical interactions.

3.5 Adsorption isotherm analysis

The influence of initial pollutant concentration on the adsorption performance is shown in **Figure 7**. As the initial concentration increased, the adsorption capacity per unit mass gradually rose, while the removal efficiency correspondingly declined. This was because the limited active sites on the adsorbent tended to become saturated at high concentrations. The isothermal adsorption data were fitted using the Langmuir and Freundlich models (**Table 2**). The results indicated that the R^2 value of the Langmuir model approached 1, suggesting that the adsorption of NH_4^+-N and PO_4^{3-}-P on the surface of Fe_3O_4@Zeolite was more inclined toward monolayer adsorption.

3.6 Thermodynamic analysis

To explore how temperature affects the adsorption process, experiments were conducted within the temper-

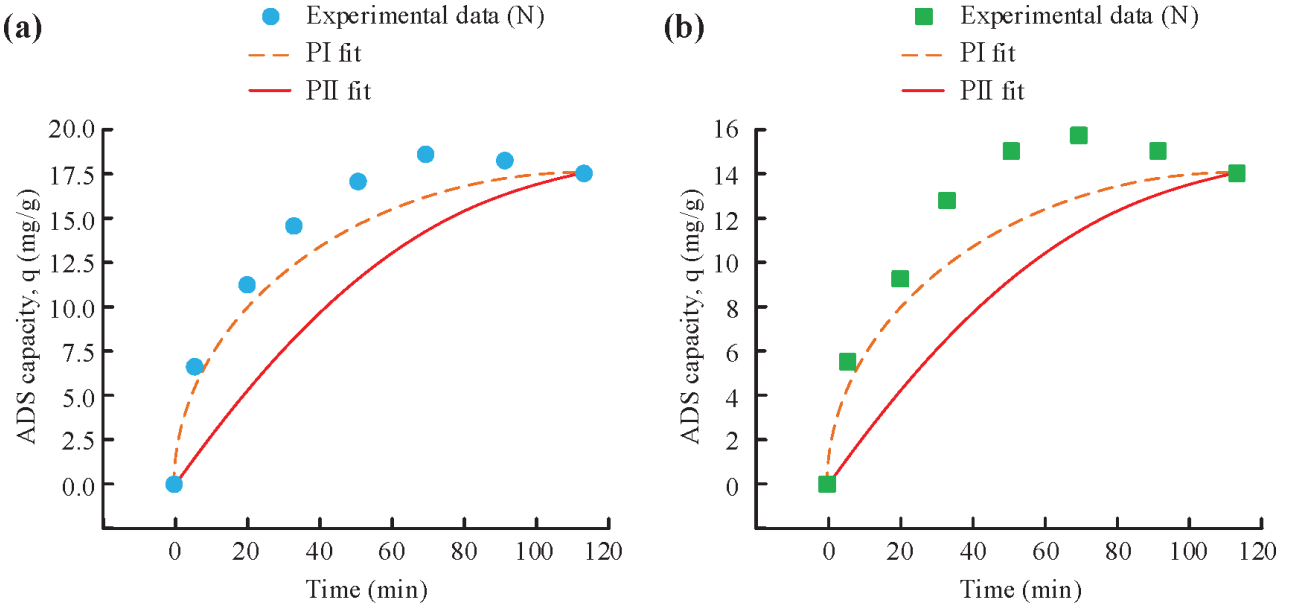

Figure 6: Adsorption kinetic curves and pseudo-second-order model fitting for: a) NH_4^+-N and b) PO_4^{3-}-P removal by Fe_3O_4@Zeolite

Table 2: Fitting parameters of adsorption kinetics and isotherm model

Adsorbate	Model	Parameters	Value	R^2
NH_4^+-N	Kinetics	q_e, exp	18.4 mg g^{-1}	–
	pseudo first order	k_1	0.056 min^{-1}	0.942
		q_e, cal	16.8 mg g^{-1}	–
	pseudo second order	k_2	0.029 g mg^{-1} min^{-1}	0.998
		q_e, cal	18.5 mg g^{-1}	–
	Isotherms	–	–	–
	Langmuir	q_m	23.5 mg g^{-1}	0.991
		K_L	1.34 L mg^{-1}	
	Freundlich	K_F	4.17 (mg g^{-1})(L mg^{-1})$^{1/n}$	0.965
		n	2.58	–
PO_4^{3-}-P	Kinetics	q_e, exp	15.9 mg g^{-1}	–
	Pseudo first order	k_1	0.048 min^{-1}	0.933
		q_e, cal	14.2 mg g^{-1}	–
	pseudo second order	k_2	0.020 g mg^{-1} min^{-1}	0.996
		q_e, cal	16.1 mg g^{-1}	–
	Isotherms	–	–	–
	Langmuir	q_m	21.6 mg g^{-1}	0.994
		K_L	1.15 L mg^{-1}	–
	Freundlich	K_F	3.89 (mg g^{-1})(L mg^{-1})$^{1/n}$	0.958
		n	2.41	–

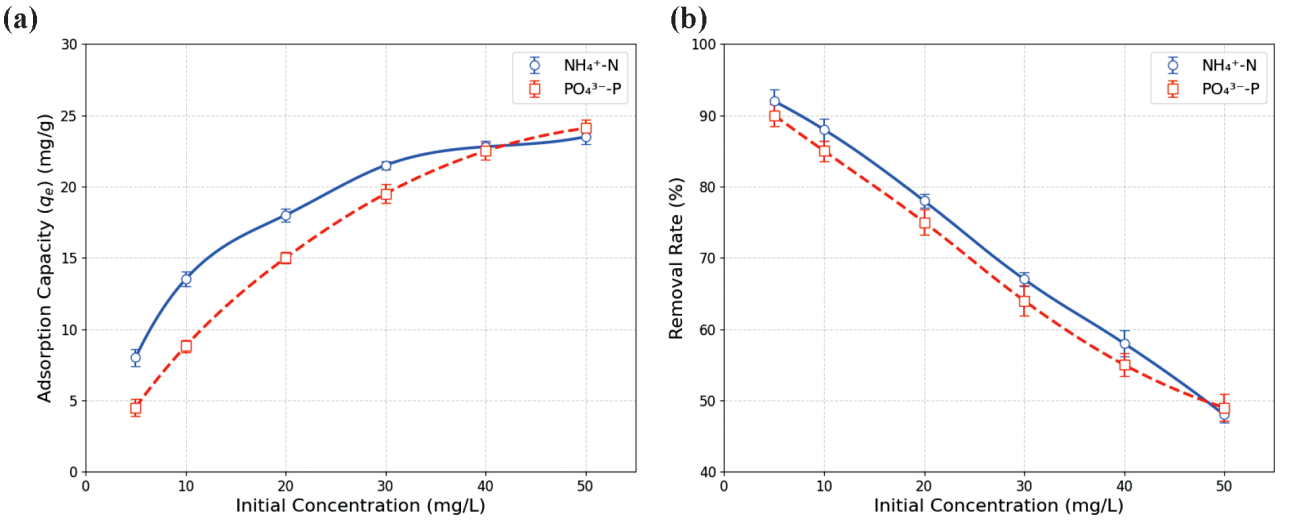

Figure 7: Effects of initial pollutant concentration on the (a) adsorption capacity and (b) removal efficiency of Fe_3O_4@Zeolite

ature range 20 to 40 °C. As shown in **Table 3**, with the increase in temperature, the equilibrium adsorption capacity rose, indicating that the adsorption was an endothermic process. According to the calculated thermodynamic parameters, the Gibbs free-energy change (ΔG°) values were all negative, suggesting that the adsorption process occurred spontaneously. The positive enthalpy change (ΔH°) confirmed the endothermic nature of the adsorption. The positive entropy change (ΔS°) implied that the adsorption led to a heightened level of disorder at the solid-liquid boundary.

Table 3: Thermodynamic parameters for the adsorption of N and P by Fe_3O_4@Zeolite

Adsorbate	T (°C)	q_e (mg g^{-1})	ΔG° (kJ mol^{-1})	ΔH° (kJ mol^{-1})	ΔS° (J (mol·K)$^{-1}$)
N	20	16.2	–10.8	22.4	+110
	30	17.5	–12.1		
	40	18.4	–13.6		
P	20	14.8	–11.2	25.1	+118
	30	16.5	–12.7		
	40	17.1	–14.3		

3.7 Influence of coexisting ions

The coexisting ions present in real wastewater contribute to ionic strength and might affect the performance of the adsorbent. To simulate this complex matrix, high concentrations of common interfering ions were introduced. As shown in **Figure 8**, the presence of ions like Ca^{2+}, Mg^{2+}, Na^+, and SO_4^{2-} all exerted a certain degree of inhibition on the adsorption process. Among them, the impact of divalent cations Ca^{2+} and Mg^{2+} was particularly significant, likely because they competed with NH_4^+ for the ion-exchange sites on zeolite. Notably, the presence of SO_4^{2-} also exhibited a slight inhibitory effect on PO_4^{3-}-P removal, with the removal efficiency decreasing from 81.2 % to 78.9 % (**Figure 8b**). This could be attributed to competitive adsorption between structurally similar SO_4^{2-} and PO_4^{3-} anions for the active hydroxyl sites (Fe-OH) on the surface of Fe_3O_4 particles. However, this inhibitory effect was relatively limited, possibly because PO_4^{3-}-P tended to form more stable inner-sphere complexes with Fe-OH, whereas sulfate mainly formed weaker outer-sphere complexes through electrostatic attraction, putting it at a disadvantage in the competition.

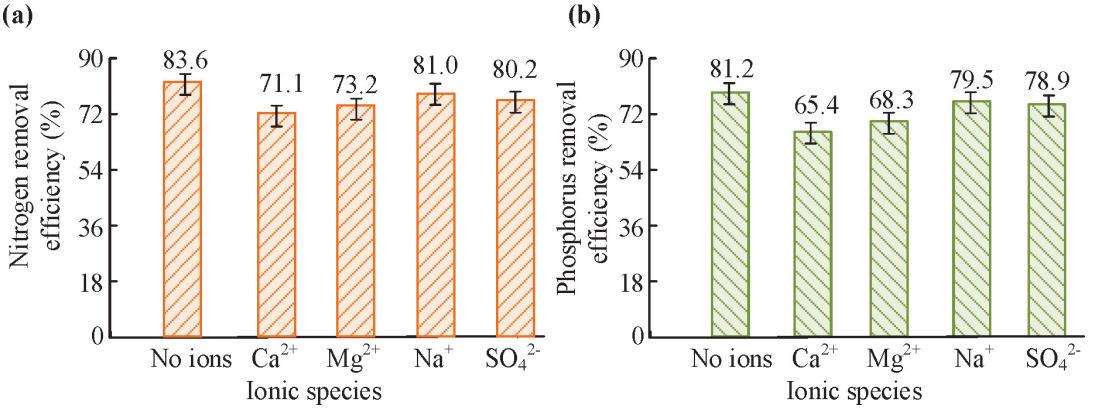

Figure 8: Impact of common coexisting ions on the efficiency of (a) NH_4^+-N and (b) PO_4^{3-}-P removal by Fe_3O_4@Zeolite

Despite this, the composite material still maintained high removal efficiencies for target pollutants in complex water bodies containing various coexisting ions, demonstrating its good potential for practical applications.

3.8 Adsorption performance of dynamic column

A fixed-bed column experiment was conducted to simulate a continuous-flow treatment scenario. As shown in **Figure 9a**, the effluent concentration exhibited a typical "S"-shaped breakthrough curve over time. At a flow rate of 8 mL min^{-1}, the breakthrough times for NH_4^+-N and P were 110 minutes and 95 min. The data were well-fitted by the Thomas model (**Figure 9b**), indicating that this model could be used to predict the performance and service life of the adsorption column.

3.9 Regeneration and stability of adsorbent

The regenerability of an adsorbent serves as a key metric for assessing its economic feasibility and sustainability. In this study, the regeneration mechanism relied on specific chemical interactions: NaCl solution was primarily used to regenerate the ion-exchange sites of the zeolite by displacing adsorbed NH_4^+ with Na^+, while NaOH and HCl solutions facilitated the desorption of phosphate from the Fe_3O_4 surface via ligand exchange and electrostatic adjustment. As shown in **Figure 10**, this composite material demonstrated exceptional regenerability. In the first adsorption-desorption cycle, the removal efficiencies of the material for NH_4^+-N and PO_4^{3-}-P were 83.6 % and 81.2 %, respectively, which were consistent with its initial performance under optimal conditions. After five consecutive cycles of use, the removal efficiencies stabilized at 74.0 % and 72.3 %, respectively. This meant that even after undergoing five rigorous regeneration processes, the retention rates of removal efficiency (i.e., the efficiency in the fifth cycle divided by that in the first cycle) for NH_4^+-N and PO_4^{3-}-P by the adsorbent still reached as high as 88.5 % and 89.0 %, respectively. This slight decline in performance could be attributed to the irreversible occupation of some active sites or a minor loss of material during the regeneration process. Overall, its excellent reusability significantly re-

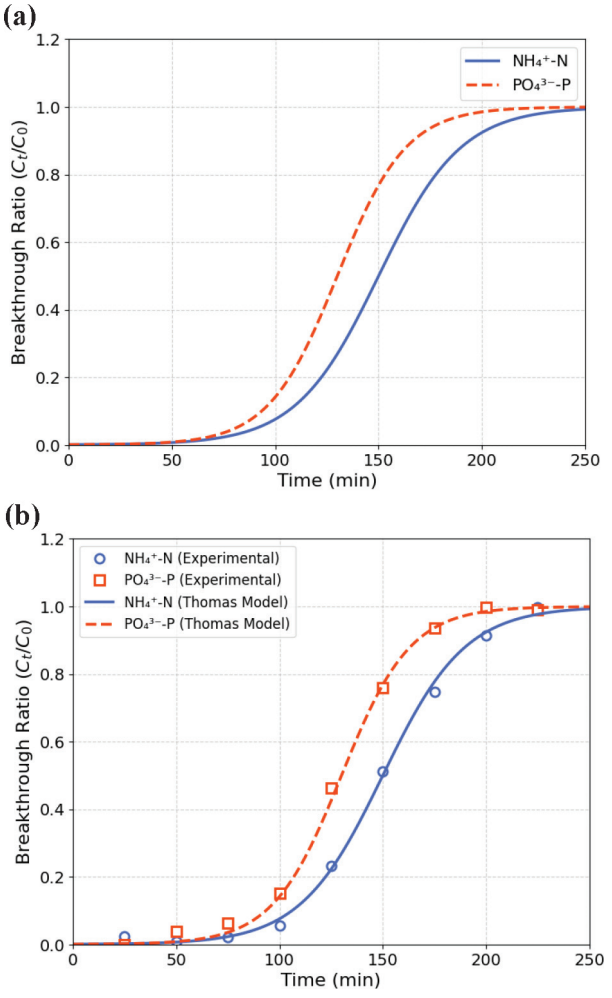

Figure 9: Results of the dynamic column experiment including: a) breakthrough curves for NH_4^+-N and PO_4^{3-}-P, b) fitting results of the Thomas model

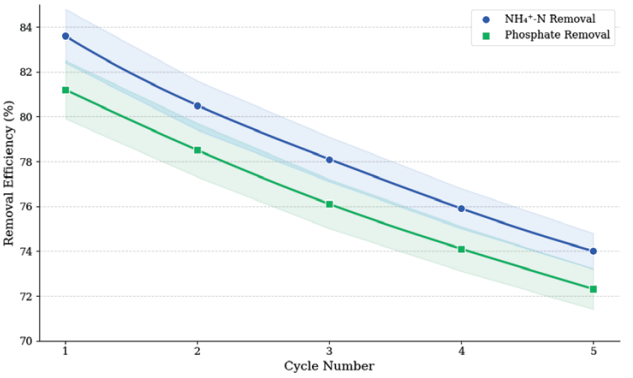

Figure 10: Regeneration performance of Fe_3O_4@Zeolite over five consecutive adsorption-desorption cycles

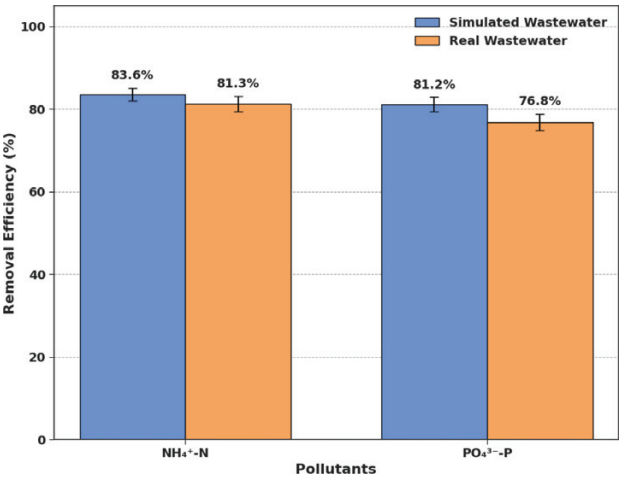

Figure 11: Comparison of the removal efficiencies of NH_4^+-N and PO_4^{3-}-P by Fe_3O_4@Zeolite between simulated wastewater and real rural sewage

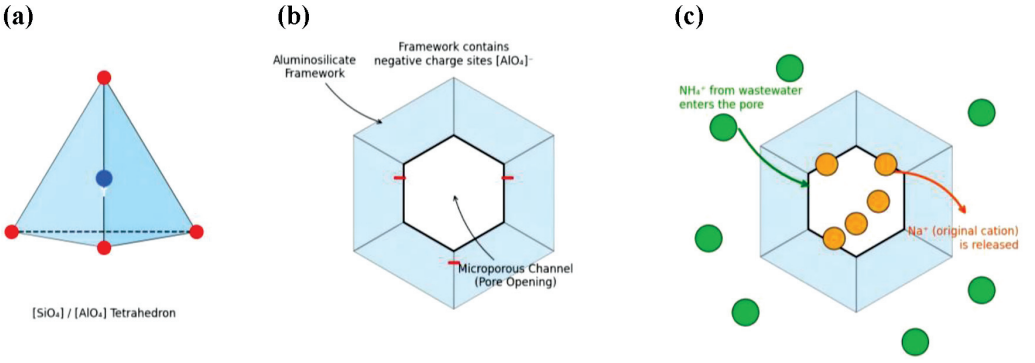

Figure 12: Diagrammatic illustration of zeolite's microstructure and the ion-exchange mechanism for NH_4^+ removal including: a) basic building unit, b) 3D framework and pores and c) ion exchange mechanism

duced potential operational costs, highlighting its great potential for sustainable engineering applications.

3.10 Application verification in real rural sewage

To further evaluate the application potential of Fe_3O_4@Zeolite in real-world environments, the study conducted verification experiments using authentic rural domestic sewage as the treatment target. As shown in **Figure 11**, the composite material still demonstrated highly efficient removal capabilities for NH_4^+-N and PO_4^{3-}-P in real water bodies with complex compositions.

Specifically, the removal rate of NH_4^+-N reached 81.3 %, showing only a slight decline compared to the removal rate in simulated wastewater (83.6 %). For PO_4^{3-}-P, the removal rate reached 76.8 %, exhibiting a certain degree of decrease compared to the 81.2 % achieved in simulated wastewater. This decline is primarily attributable to the complex matrix of real sewage. As indicated in **Table 1**, the real sewage contained a high background concentration of sulfate (95.8 mg L^{-1}). Consistent with the interference results in Figure 8b, these high concentrations of sulfate ions compete with phosphate for surface binding sites on the Fe_3O_4 nanoparticles via electrostatic attraction. Additionally, dissolved organic matter (DOM) and carbonate ions likely contributed to the competitive inhibition. Despite this, the composite material was still able to remove more than 75 % of PO_4^{3-}-P and 80 % of NH_4^+-N.

This result strongly demonstrated that the Fe_3O_4@Zeolite composite material possessed excellent substrate selectivity and anti-interference ability. Its "synergistic dual-site mechanism" remained robust and effective in complex water environments, thereby confirming its immense application prospects in treating actual rural sewage.

4 DISCUSSION

4.1 Synergetic adsorption mechanism: an efficient "synergistic dual-site" mode

This study confirmed that the high efficiency of Fe_3O_4@Zeolite stemmed from an ingenious "synergistic dual-site mechanism". The chemisorption nature of this mechanism had been revealed by kinetic and thermodynamic data. A more in-depth chain of evidence was integrated as follows: First, the pH-dependent experiments (**Figure 5**) clarified the assignment of functional units – the zeolite framework was responsible for NH_4^+ removal, while Fe_3O_4 nanoparticles served as the sole active center for PO_4^{3-}-P removal. This finding decisively demonstrated that different components of the composite material undertook distinct adsorption tasks. Second, XPS analysis (**Figures 4f** and **4g**) revealed the chemical nature of this process at the atomic scale, namely, that PO_4^{3-} formed stable Fe-O-P inner-sphere surface complexes through ligand exchange with hydroxyl groups on the surface of Fe_3O_4.

On the whole, the entire synergistic process could be described as follows: On the porous zeolite framework, the net negative charges generated by the substitution of $[SiO_4]$ tetrahedra with $[AlO_4]$ tetrahedra efficiently captured NH_4^+ through electrostatic attraction and ion exchange. Specifically, the exchangeable cations (such as Na^+, K^+) in the zeolite channels and cages, which were used to balance the charges, were stoichiometrically replaced by NH_4^+ ions in water (**Figure 12**). Meanwhile, the uniformly dispersed Fe_3O_4 nanoparticles on its surface utilized their abundant surface hydroxyl sites (Fe-OH) as exclusive "anchor points" to chemically complex with PO_4^{3-}-P ions. It was precisely this structural integration that allowed for a spatial separation of the active sites: the internal pore channels of the zeolite framework sequestered NH_4^+ cations, while the external Fe_3O_4 nanoparticles captured PO_4^{3-} anions. This design effectively minimized steric hindrance and direct competition between the two pollutants, allowing distinct adsorption processes to occur simultaneously without significant mutual interference.

4.2 Performance comparison and application prospect

To objectively evaluate the performance of this material, the study compared it with other adsorbents mentioned in recent studies (**Table 4**).

Table 4: Comparison of adsorption properties of NH_4^+-N and PO_4^{3-}-P between this research material and other adsorbents

Adsorbent	NH_4^+-N q_m (mg g^{-1})	PO_4^{3-}-P q_m (mg g^{-1})	Separation mode	Raw material cost	Reference
Fe_3O_4@Zeolite (This work)	23.5	21.6	Magnetic separation	Low	Not applicable
Magnesium modified bentonite	6.8	41.5	Filtration/centrifugation	High	Sun et al., 2025 [23]
Sodium alginate-doped carbon dot composite hydrogel	4.5	24.3	Filtration/centrifugation	High	et al., 2023 [24]
Original Zeolite	12.1	≈0	Filtration/centrifugation	Low	et al., 2024 [25]
Magnesium-modified biochar	28.9	Not applicable	Filtration/centrifugation	Middle	Sürmeli et al., 2025 [26]

(Note: in the table, "not applicable" means that the material is not studied or invalid for this pollutant; "≈0" means that the adsorption capacity is very low and can be ignored)

As seen from **Table 4**, some adsorbents specialized for single-pollutant removal, such as magnesium-modified bentonite, exhibited higher adsorption capacities for PO_4^{3-}-P.[23] This is primarily attributed to the specific affinity of magnesium-based materials for phosphate ions. However, these materials generally lack the capability to effectively remove NH_4^+-N, and their powder form often necessitates complex filtration or centrifugation steps for separation.

In contrast, the core advantage of the Fe_3O_4@Zeolite developed in this study lies not in pursuing the ultimate adsorption capacity for a single pollutant, but in its balanced simultaneous removal performance and engineering practicality. While specialized single-pollutant adsorbents may achieve higher capacities, they often lack the versatility required for complex sewage containing both N and P. The distinct advantages of this composite are summarized as follows:

(1) Dual-function balance: By utilizing inexpensive and readily available iron salts and natural zeolite, it achieved balanced and efficient simultaneous removal of two major nutrient salts, which is crucial for practical wastewater treatment.

(2) Cost-effectiveness: The raw materials are widely sourced and inexpensive, and the preparation method (hydrothermal method) is simple, facilitating easy large-scale production and better meeting economic requirements.

(3) Engineering applicability: Its excellent magnetic separation properties greatly simplify the solid-liquid separation process, eliminating the need for complex filtration or sedimentation units and perfectly fitting the decentralized, low-maintenance wastewater treatment scenarios in rural areas.

5 CONCLUSION AND PROSPECTS

5.1 Conclusion

In summary, this study successfully developed a structurally stable and high-performing Fe_3O_4@Zeolite bifunctional magnetic adsorbent and confirmed that, through the synergistic dual-site mechanism involving zeolite ion exchange and Fe_3O_4 surface complexation, it achieved efficient and simultaneous removal of NH_4^+-N and PO_4^{3-}-P from water bodies. The key findings are outlined below:

1. Successful construction and characterization: Fe_3O_4 nanoparticles were successfully and uniformly loaded onto the zeolite framework, forming a stable magnetic composite structure.
2. Exceptional simultaneous removal performance: Under neutral conditions (pH 6-7), the material exhibited optimal adsorption performance, with max Langmuir adsorption capacities of 23.5 mg g^{-1} for NH_4^+-N and 21.6 mg g^{-1} for PO_4^{3-}-P.
3. Clear synergistic adsorption mechanism: The adsorption process was spontaneous and endothermic chemisorption, following pseudo-second-order kinetics and the Langmuir model. Mechanistic studies clarified the synergistic removal pathways, with NH_4^+-N removed via ion exchange and PO_4^{3-}-P via surface complexation.
4. High potential for practical applications: In real rural domestic sewage, the composite material also demonstrated efficient removal capabilities for NH_4^+-N and PO_4^{3-}-P, confirming its robustness and practical feasibility in complex water environments.
5. Excellent regeneration and stability: The material exhibited outstanding regeneration ability and magnetic separation properties, with adsorption efficiency remaining above 88 % after five cycles, demonstrating significant potential for sustainable applications.

5.2 Research limitations and prospects

Despite the positive results achieved in this study, to facilitate the practical application of this technology, future research should be deepened in the following directions:

1. Long-term stability and environmental adaptability: This study has preliminarily validated the effectiveness of the composite material in static treatment of real wastewater. Future research urgently needs to build on this foundation by conducting long-term dynamic column experiments to systematically evaluate

the long-term fouling effects of coexisting organic matter (Organic Fouling) and microorganisms (Biofouling). Furthermore, given the findings in Section 3.6 that the adsorption is an endothermic process, particular attention should be paid to the adsorption kinetics and thermodynamics under low-temperature conditions (e.g., < 10 °C, typical of winter in rural China) to assess potential efficiency challenges and optimize operational parameters for cold environments.

2. Large-scale preparation and techno-economic analysis: Future research should focus on optimizing preparation processes at the pilot scale, exploring more energy-efficient and high-yield synthesis routes (e.g., microwave-assisted hydrothermal methods), and conducting comprehensive techno-economic assessments to accurately calculate material costs, operational energy consumption, and regeneration expenses in engineering applications.
3. Green regeneration processes and wastewater resource recovery: More environmentally friendly and efficient regeneration methods should be explored, such as electrochemically assisted desorption or in-situ regeneration technologies driven by microbial fuel cells, to minimize chemical consumption and secondary pollution. Additionally, investigating the potential for recovering N and P enriched in regenerated wastewater as liquid fertilizers is crucial for achieving full-process sustainability.
4. Functional expansion and upgrading of materials: Exploring the doping of other transition metal elements (e.g., Mn, Ce) can endow the composite material with catalytic oxidation activity (e.g., Fenton-like) while maintaining its N and P adsorption capacity, enabling it to degrade refractory organic micropollutants in water and achieving a functional upgrade from "nutrient removal" to "collaborative pollutant purification."

Acknowledgment

This work was supported by the Research Project Funding (2022XX(83)-002) of the Shanghai Investigation, Design & Research Institute Co., Ltd.

6 REFERENCES

[1] J. Tian, J. Y. Ji, Z. Q. Liu, J. Huang and W. T. Xue, Effect evaluation of decentralized domestic sewage treatment facilities in rural areas – a case study of Nantong City, China, Water Sci. Technol., 88 (**2023**) 3, 711–722, doi:10.2166/wst.2023.208

[2] X. F. Chen, L. Q. Chao, Y. L. Wan, X. Y. Wang and X. C. Pu, Study of the characteristics of pollutants in rural domestic sewage and the optimal sewage treatment process: a Chengdu Plain case study, Water Sci. Technol., 87 (**2023**) 9, 2373–2389, doi:10.2166/wst.2023.139

[3] J. J. Lan, L. L. Liu, X. Wang, X. X. Wu and Z. P. Wang, DOM tracking and prediction of rural domestic sewage with UV-vis and EEM in the Yangtze River Delta, China, Environ. Sci. Pollut. R., 29 (**2022**) 49, 74579–74590, doi:10.1007/s11356-022-20979-4

[4] G. Insel, G. Yilmaz, F. Hazi and N. Artan, Model-based evaluation of simultaneous nitrification and denitrification in aerobic granular sludge systems, Environ. Sci. Pollut. R., 30 (**2023**) 60, 124780–124789, doi:10.1007/s11356-023-25252-w

[5] F. Yin, S. Fukutani, M. Toyama, T. Yamamura and T. Suzuki, Radium separation from thorium and manufacturing of targets by precipitation method, J. Radioanal. Nucl. Chem., 333 (**2024**) 11, 6039–6046, doi:10.1007/s10967-024-09496-5

[6] M. A. M. Alzaky, S. S. E. Ahmed, R. A. Basheer, R. Siddig, T. A. Ibraheem, M. Kashif, F. K. Wang, H. Y. Lu, J. Y. Tan and D. X. Li, Yellow phosphorus and Potash for SOX and NOX removal, Environ. Technol., 43 (**2022**) 25, 3993–4001, doi:10.1080/09593330.2021.1939431

[7] Y. Ma, J. Y. Hu, K. Fan, W. Chen, S. C. Han, Q. M. Wu, Y. H. Ma, A. M. Zheng, E. Kunkes, T. De Baerdemaeker, A. N. Parvulescu, N. Bottke, T. Yokoi, D. E. De Vos, X. J. Meng and F. S. Xiao, Design of an Organic Template for Synthesizing ITR Zeolites under Ge-Free Conditions, J. Am. Chem. Soc., 145 (**2023**) 31, 17284–17291, doi:10.1021/jacs.3c04652

[8] K. K. Razmakhnin, Development and Justification of Treatment and Modification Technology for East Transbaikalia Zeolite Rocks, J. Min. Sci., 57 (**2021**) 3, 493–501, doi:10.1134/s1062739121030145

[9] V. V. Golovko, V. A. Kostin and V. V. Zhukov, Influence of Nanomodification on the Microstructure of the Metal of Welded Joints of Low-Alloy Steels, Mater. Sci., 59 (**2024**) 6, 762–769, doi:10.1007/s11003-024-00838-y

[10] W. Y. Zhang and E. P. C. Lai, Chemical Functionalities of 3-aminopropyltriethoxy-silane for Surface Modification of Metal Oxide Nanoparticles, Silicon, 14 (**2022**) 12, 6535–6545, doi:10.1007/s12633-021-01477-7

[11] R. F. Nafchi, R. Ahmadi, M. Heydari, M. R. Rahimipour, M. J. Molaei and L. Unsworth, In Vitro Study: Synthesis and Evaluation of Fe_3O_4/CQD Magnetic/Fluorescent Nanocomposites for Targeted Drug Delivery, MRI, and Cancer Cell Labeling Applications, Langmuir, 38 (**2022**) 12, 3804–3816, doi:10.1021/acs.langmuir.1c03458

[12] B. Q. Gao, Y. Feng, X. M. Chen and J. Zhang, A new PLA-Tween composited drug-carrying C_{60}-Fe_3O_4 multifunctional ultrasound contrast agent based on three kinds of lesions, RSC Adv., 11 (**2021**) 49, 31015–31029, doi:10.1039/d1ra04936d

[13] Y. G. Chen, Q. Chen and M. A. Chen, Influence of 3-aminopropyltriethoxysilane/tetraethylorthosilicate mixture pretreatment on the microstructure and corrosion resistance of zeolite coating, Surf. Eng., 39 (**2023**) 5, 625–635, doi:10.1080/02670844.2023.2240565

[14] T. H. Gonsalves, M. K. G. Channabasappa, R. M. Rangarasaiah and S. Joladarashi, Dynamic characterization of hybrid composite material of rotor-bearing support system, Mech. Adv. Mater. Struc., 29 (**2022**) 16, 2342–2357, doi:10.1080/15376494.2020.1861667

[15] B. S. Wee, M. F. Maligan, S. F. Chin, M. S. Elias and N. Shirai, Adsorption of U(VI) ions using functionalized sago hampas: kinetics, isotherms, and thermodynamics studies, J. Radioanal. Nucl. Chem., 333 (**2024**) 6, 2679–2689, doi:10.1007/s10967-024-09489-4

[16] A. K. Rakishev, M. D. Vedenyapina, S. A. Kulaishin and D. Kurilov, Adsorption of Salicylic Acid from Aqueous Solutions on Microporous Granular Activated Carbon, Solid Fuel Chem., 55 (**2021**) 2, 117–122, doi:10.3103/s0361521921020063

[17] Y. Liu, L. J. Xia, H. Guo, A. M. Wang, J. B. Hu, W. Zhang, W. L. Xu and Y. L. Wang, Kinetics and Thermodynamics Studies of Cationic Dye Adsorption onto Carboxymethyl Cotton Fabric, J. Nat. Fibers, 19 (**2022**) 1, 173–184, doi:10.1080/15440478.2020.1731908

[18] S. N. Taqui, C. S. Mohan, B. A. Khatoon, M. E. M. Soudagar, T. M. Y. Khan, M. A. Mujtaba, W. Ahmed, A. Elfasakhany, R. Kumar and C. I. Pruncu, Sustainable adsorption method for the remediation of malachite green dye using nutraceutical industrial fenugreek seed spent, Biomass Convers. Bior., 13 (**2023**) 10, 9119–9130, doi:10.1007/s13399-021-01827-w

[19] G. Özsin and E. A. Varol, Potential of microwave-assisted hydrothermal modification for enhanced fly ash adsorption capacity toward to

heavy metals: A comprehensive investigation of adsorbent characterization, isotherms, kinetics, and thermodynamics, Sep. Sci. Technol., 59 (**2024**) 1, 71–86, doi:10.1080/01496395.2024.2315611

[20] Q. Z. Zhai, Study on adsorption of methylene blue by modified peanut shell: adsorption kinetics, thermodynamics, isotherm properties, Chem. Eng. Commun., 211 (**2024**) 4, 633–646, doi:10.1080/00986445.2023.2255533

[21] M. Shigei, R. B. Herbert, F. Persson, E. Sokolova and S. S. Dalahmeh, Efficient removal of organic matter and nitrogen from municipal wastewater in multi-module biochar filters for onsite wastewater treatment, Environ. Technol., 46 (**2025**) 9, 1531–1543, doi:10.1080/09593330.2024.2402096

[22] T. T. Dezfouli, M. Kashefiolasl, R. Marandi, M. Emtyazjoo and M. Javaheri, Carbon Aerogel Coated Air-Cathode Bioelectrochemical System for Simultaneous Nitrogen and Phosphorus Removal, Iran. J. Chem. Chem. Eng. Int. E. Edit., 40 (**2021**) 5, 1431–1445, doi:10.30492/ijcce.2020.43236

[23] Q. Sun, J. H. Yuan, Z. Y. Yang, Q. Q. Shen, X. P. Hou, M. Zhang, Y. Q. Wu, C. Y. Zhong and D. Xu, Optimized preparation, characterization and the adsorption mechanism of magnesium-modified bentonite-based porous adsorbents: thermodynamic and kinetic analysis, New J. Chem., 49 (**2025**) 12, 4982–5001, doi:10.1039/d4nj04076g

[24] X. Zhang, S. W. Luo, J. X. Duan, T. Lan and Y. Wei, Fabrication of sodium alginate-doped carbon dot composite hydrogel and its application for La (III) adsorption and enhanced the removal of phosphorus, Environ. Sci. Pollut. R., 30 (**2023**) 49, 108230–108246, doi:10.1007/s11356-023-29958-9

[25] X. R. Zhou, X. L. Han, Z. Y. Qu, J. X. Zhang, F. Zeng, Z. C. Tang and R. Z. Chen, Hierarchical FAU Zeolites Boosting the Hydrocracking of Polyolefin Waste into Liquid Fuels, ACS Sustain. Chem. Eng., 12 (**2024**) 15, 6013–6022, doi:10.1021/acssuschemeng.4c01097

[26] R. Sürmeli, Ö. Madenli, A. Bayrakdar, E. Deveci and B. Calli, Phosphate recovery from digestate using magnesium-modified fungal biochar, Clean Technol. Envir. Policy, 27 (**2025**) 8, 3557–3571, doi:10.1007/s10098-024-03035-2